

Small-angle neutron scattering study of micropore collapse in amorphous solid water

Supporting Information:

Spherical pore shape and Maxwellian pore size distribution:

In addition to the new Guinier-Porod model we have also tried to fit our data by a model assuming a spherical pore shape and a Maxwellian pore size distribution as described by Shull et al. (C. G. Shull, and L. C. Roess, J. Appl. Phys. **18**, 295 (1947)).

Shull et al. derived the following expression for the small angle scattering intensity I as a function of the magnitude of the scattering vector Q for polydisperse pores.

$$I(Q) = C \cdot \int_0^{\infty} N(r) \cdot V^2(r) \cdot F(Q, r) dr \quad (1)$$

For a porous media, $N(r)$ corresponds to the pore size distribution, $V(r)$ is the pore volume and C a scaling factor. The information about the pore shape is embedded in the form factor $F(Q, r)$. In the case of a Maxwellian pore size distribution, $N(r)$ has the form;

$$N(r) = \sqrt{\frac{2}{\pi}} \cdot \frac{r^2}{\sigma^3} \cdot \text{Exp}\left(-\frac{r^2}{2\sigma^2}\right) \quad (2)$$

Shull et al. approximated the form factor for spherical pores at small angles by the Guinier approximation with $r_G = \sqrt{3/5} \cdot r$ the radius of gyration of a sphere.

$$F(Q, r) \approx \text{Exp}\left(-\frac{Q^2 \cdot r_G^2}{3}\right) = \text{Exp}\left(-\frac{Q^2 \cdot r^2}{5}\right) \quad (3)$$

By inserting equations (2), (3) together with the volume of a sphere into expression (1) integrating it, and using the scaling factor K we get

$$I(Q) = \frac{K}{\sigma^3} \cdot \left(\frac{Q^2 \cdot \sigma^2}{5} + \frac{1}{2}\right)^{-\frac{9}{2}} \quad (4)$$

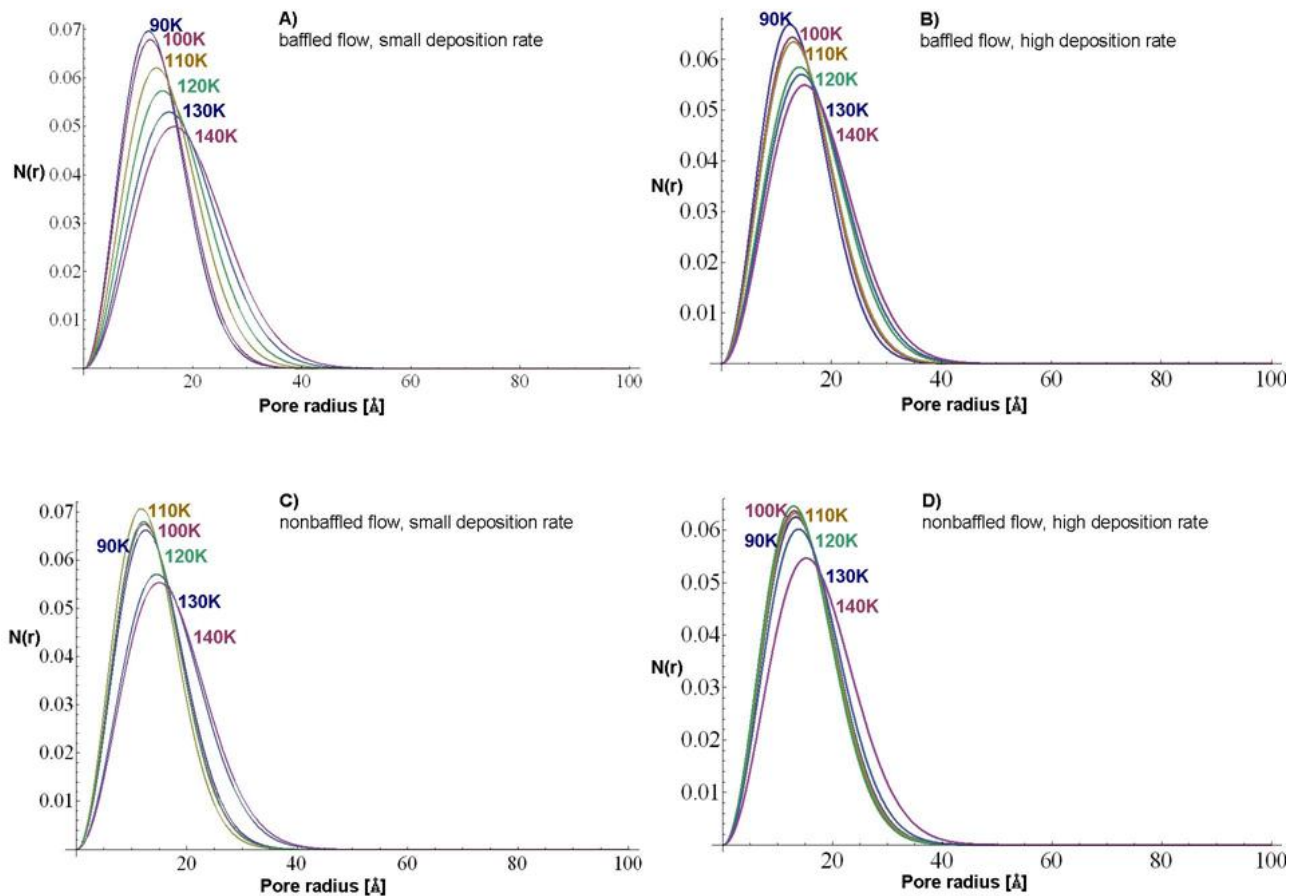
which forms the basis for our data analysis.

The fitting process was performed with the data evaluation program Origin Pro 7.5G. However, using the approximation of spherical pores the fit of the model to the data does not indicate collapse of micropores. Instead, a continuous increase in average pore radius from about 15 Å to 20 Å and a slight increase in the width of the Maxwellian distribution at 90–140 K produce the best fit to all four data sets (see Figure below).

In general the morphology of the micropores in ASW is not known (V. Buch and J. P. Devlin, Water in Confining Geometries (page 368), Springer Berlin Heidelberg New York (2003)), the possibility of interconnected pores is not excluded (G. A. Kimmel et al.; JCP **114**, 5284 (2001) and G. A. Kimmel et al.; JCP **114**, 5295 (2001)). The necessity of a pore collapse is well known from many previous studies on ASW samples. Ice grown at 70–80 K is known as compact ASW with micropores that are inaccessible to adsorbate molecules. If however the ice is formed at 10 K with adsorbates such as CO and N₂, we can probe the pore sizes and distribution all the way to

the crystallisation. With these adsorbates the pores may or may not aggregate (thereby becoming larger in volume and less frequent) or simply collapse and disappear (crystalline ice has no pores – indeed as shown by this work). Adsorbate desorption studies clearly show that gas is liberated at a constant rate suggesting that pores do not aggregate and become fewer in number whilst increasing in volume – rather the pores decrease in volume and the number gradually also tends to zero. This is corroborated by the data presented here. Under the assumption that the increase in intensity of the $1/Q$ data is enhanced over the power law scattering in the pore region, due to free space path length of the scattered neutrons, then if the pores got BIGGER but FEWER we would expect the hump position to (a) change peak position – which it does not and (b) increase in intensity as the path length of the scattered neutrons increases again. If however the pores simply shrink in number then the hump will gradually disappear. This is exactly what happens here and is entirely commensurate with data from other ASW experiments. That is, in order to capture the physics of pore-collapse the spherical pore approximation is inconsistent with the experimental data and so needs to be revised or replaced. For this reason we have resorted in modelling our data by the Guinier-Porod model in the main manuscript.

Supporting Figures:

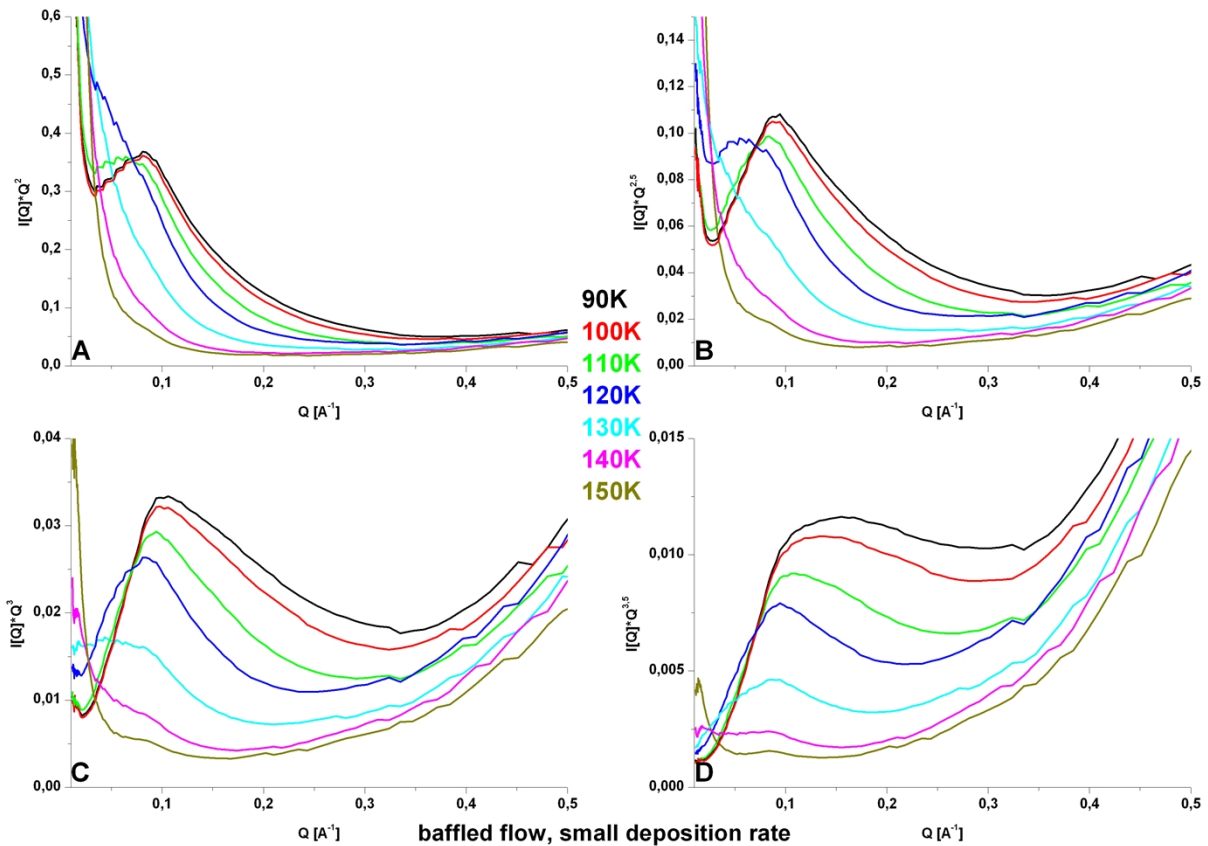


Temperature evolution between 90 and 140 K of Maxwell pore size distribution for spherical pore shape

A) baffled flow, small deposition rate B) baffled flow, high deposition rate C) non-baffled flow, small deposition rate D) non-baffled flow, high deposition rate.

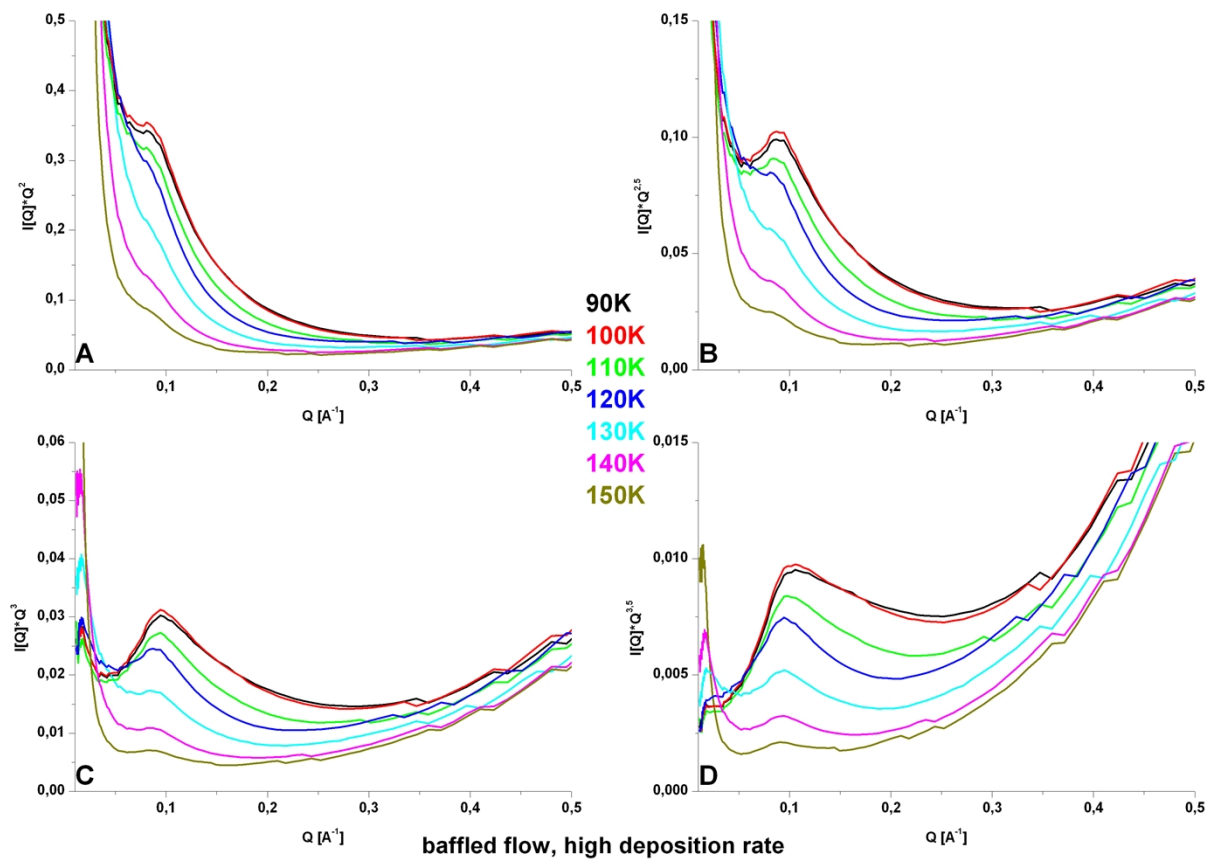
Standard linear plots $I(Q)*Q^d$ versus Q :

The following figures contain the standard linear plots $I(Q)*Q^d$ versus Q with different values for d for all four samples investigated in this study. In the main part of the paper the exponent d is chosen in a way that the “hump” at $Q=0.1 \text{ \AA}^{-1}$ in the scattered intensity develops into a pronounced peak (compare figure 4).

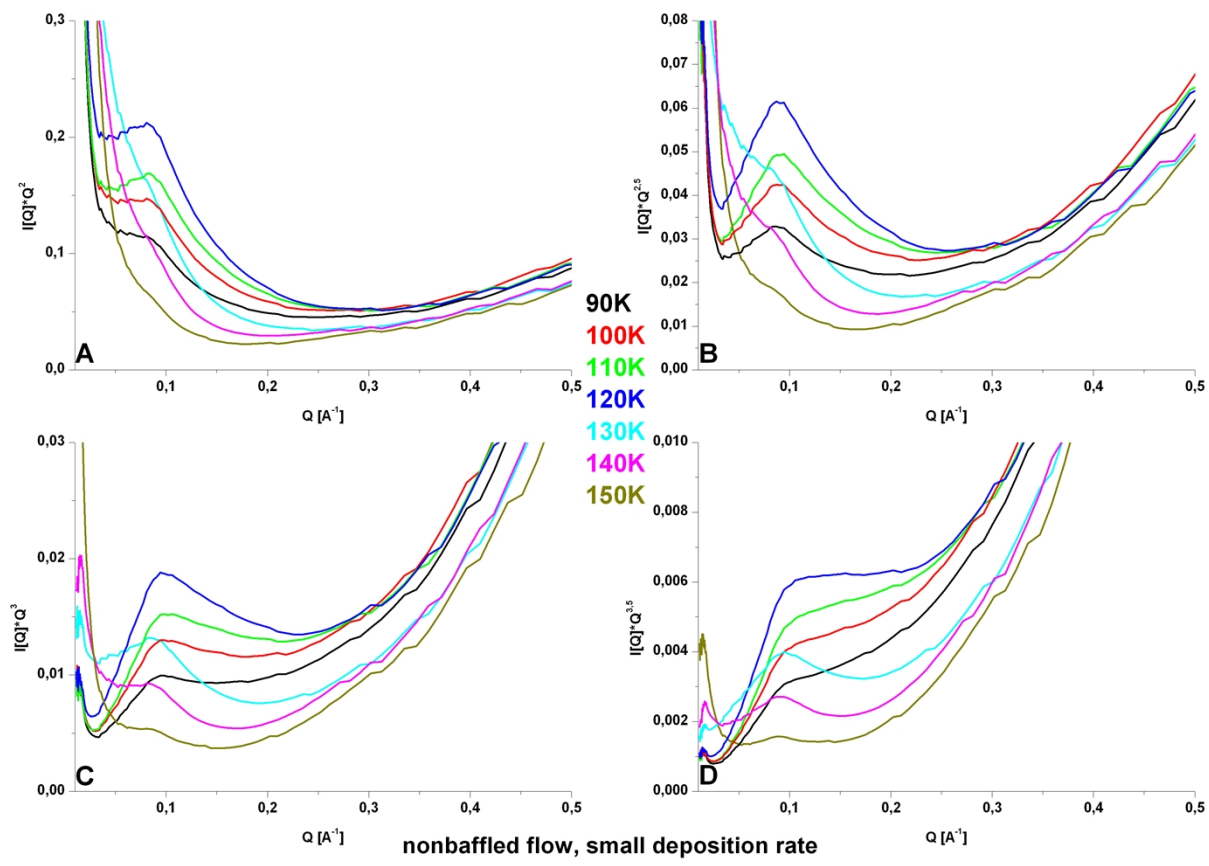


Temperature evolution between 90 and 150 K of standard linear plots $I(Q)*Q^d$ versus Q with d between 2 and 3,5 for the baffled flow, small deposition rate sample.

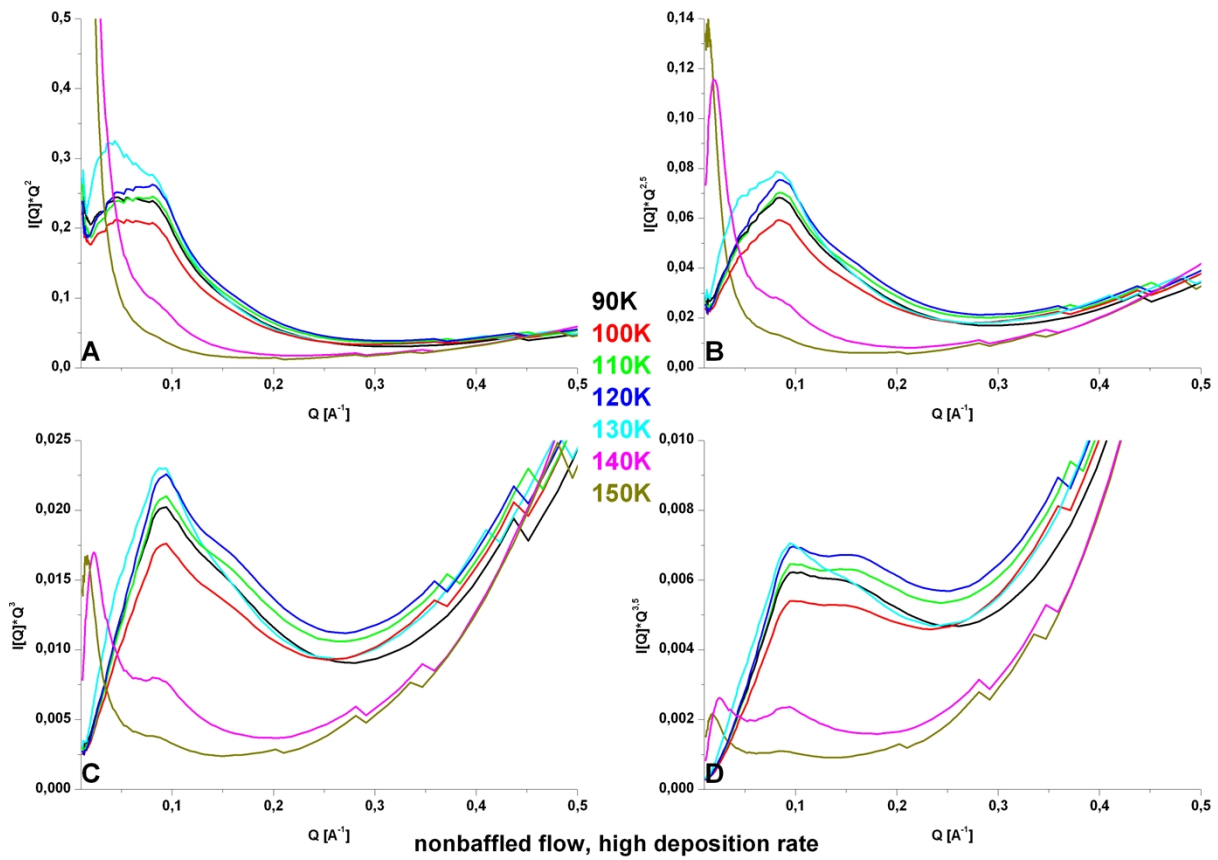
A) $d=2$ B) $d=2,5$ C) $d=3$ D) $d=3,5$



Temperature evolution between 90 and 150 K of standard linear plots $I(Q)*Q^d$ versus Q with d between 2 and 3,5 for the baffled flow, high deposition rate sample.
 A) $d=2$ B) $d=2,5$ C) $d=3$ D) $d=3,5$



Temperature evolution between 90 and 150 K of standard linear plots $I(Q)*Q^d$ versus Q with d between 2 and 3,5 for the nonbaffled flow, small deposition rate sample.
 A) $d=2$ B) $d=2,5$ C) $d=3$ D) $d=3,5$



Temperature evolution between 90 and 150 K of standard linear plots $I(Q) \cdot Q^d$ versus Q with d between 2 and 3,5 for the baffled flow, small deposition rate sample.
 A) $d=2$ B) $d=2,5$ C) $d=3$ D) $d=3,5$

